

How Asian slum emissions impact local microclimates in polluted air masses

Satyajit Ghosh^{1,2}  | C. R. Sathish Kumar³ | Siddharth Gumber¹  | Steven Dobbie² | Huiyi Yang⁴

¹Department of Thermal and Energy Engineering, School of Mechanical Engineering, Vellore Institute of Technology, Vellore, Tamil Nadu, India

²School of Earth and Environment, University of Leeds, Leeds, UK

³Tamil Nadu Pollution Control Board, Chennai, Tamil Nadu, India

⁴Livelihoods and Institutions Department, Natural Resources Institute, University of Greenwich, Chatham, UK

Correspondence

Satyajit Ghosh, Department of Thermal and Energy Engineering, School of Mechanical Engineering, Vellore Institute of Technology, Vellore 632014, Tamil Nadu, India.

Email: satyajitg@vit.ac.in

Funding information

ERASMUS+ Capacity Building Scheme for Higher Education

Abstract

Urban sprawl comprising densely populated slums over South Asian cities yields copious amounts of soot and black carbon from archaic cooking methods involving cow dung cakes and firewood, which remain afloat for over 10–12 h, enabling them to *age* in a sulphur rich environment. Not only are there toxicological concerns arising out of improper ventilation mechanisms, but there are also other concerns impacting the local microclimate. These emissions mix with other aerosol particles and, when conditions are favourable, are rendered partially soluble, enabling them to activate into cloud condensation nuclei. This study first yields a quantification of the soluble mass fraction and subsequently shows how aerosols from this local area source mix with background aerosol modes to perturb the local cloud microphysics over Chennai, a megacity in Southern India. On-site sampling was undertaken to find the mass concentrations of the collected deposits separately from cow dung and firewood fuel. Additional micro-physical attributes, including the morphological indentations that served as a receptacle to contain the accreted sulphate along with the particle size distribution were ascertained through Scanning Electron Microscopy. It is shown that accreted sulphate on carbonaceous particles facilitates CCN activation over the city. We show through large-eddy simulations (LES) that extensive slum emissions over the study region contribute to the observed local cloud cover and enhanced rain amounts over a densely built-up area housing the city's most vulnerable citizens.

KEYWORDS

accreted sulphate, Asian slums, black carbon, cloud microphysics, local microclimate, particulate matter toxicology

This is an open access article under the terms of the [Creative Commons Attribution](https://creativecommons.org/licenses/by/4.0/) License, which permits use, distribution and reproduction in any medium, provided the original work is properly cited.

© 2022 The Authors. *Atmospheric Science Letters* published by John Wiley & Sons Ltd on behalf of the Royal Meteorological Society.

1 | INTRODUCTION

The progression of industrialisation and urbanisation in India is directly linked to the levels of air pollution, and its cities are among the most polluted in the world, receiving pollutants from vehicles, industries and power plants (Guttikunda & Kopakka, 2014; US EPA, 2012; Sharma

et al., 2010; Ghanti and Ghosh, 2010). It is not only urban areas that are facing the brunt of air pollution but also rural settlements because of primitive cooking methods using biomass (see Figure 1; Rehman et al., 2011). The infamous Indo-Asian haze, also known as atmospheric brown clouds, consists of layers of air pollutants with a mixture of organic carbon, black carbon and dust along

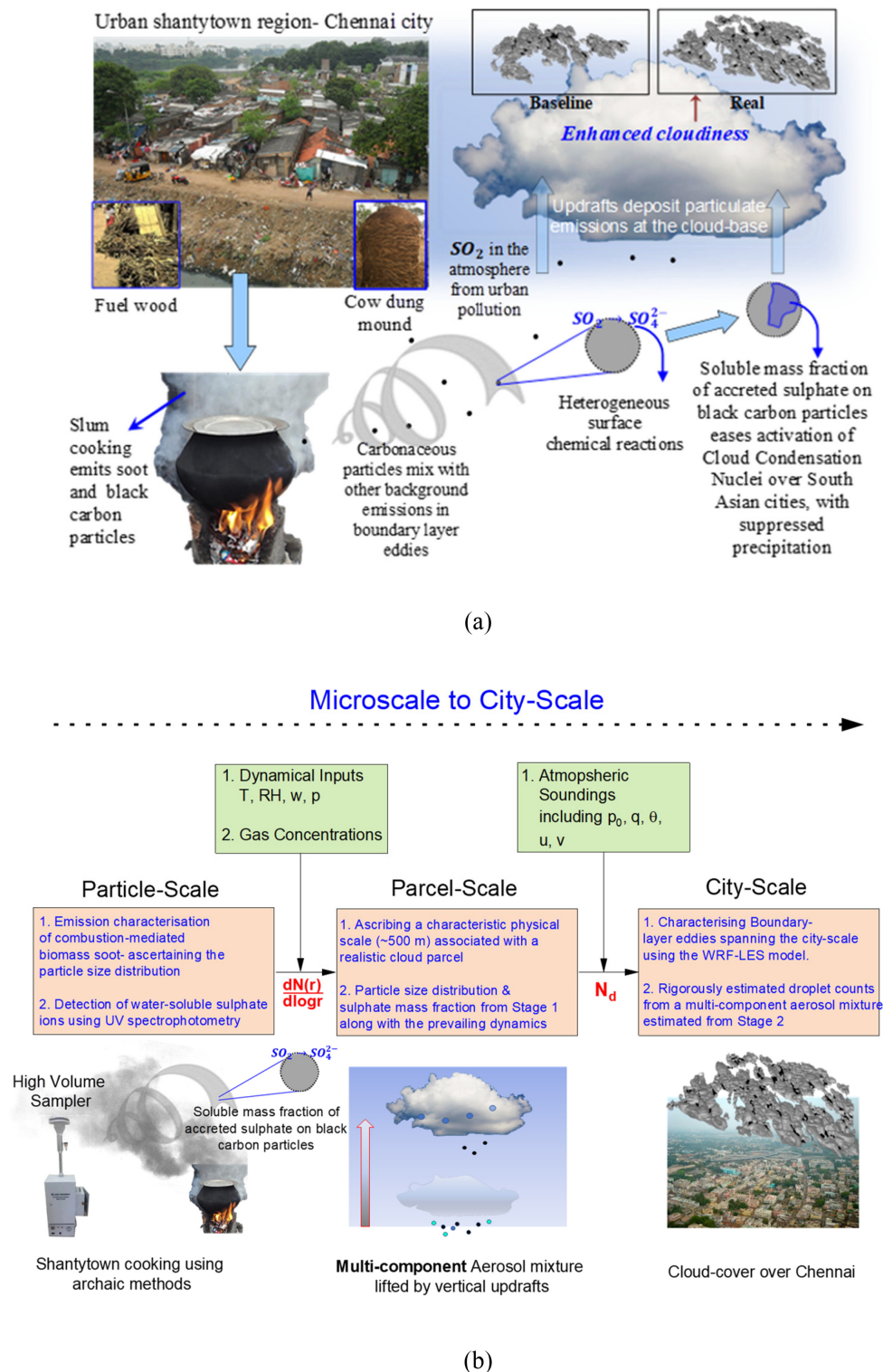


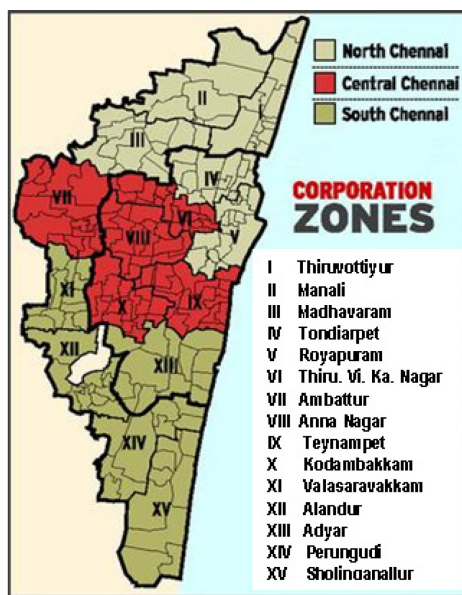
FIGURE 1 (a) Cook stove emissions over urban sprawl in South India and expected microphysical implications. Burning of Bio and fossil fuels is the main contributor of carbonaceous aerosol particles over the region. (b) Schematic diagram illustrating the coupling of microscale processes at the particle level, parcel-scale and boundary layer processes. Combustion-mediated soot and black carbon from biomass burning in shantytowns modulate the local cloud cover

with local slum emissions (Padmakumari et al., 2013). This layer can absorb and scatter solar radiations and impact climate and hydrological cycles over South Asia (Ding et al., 2021).

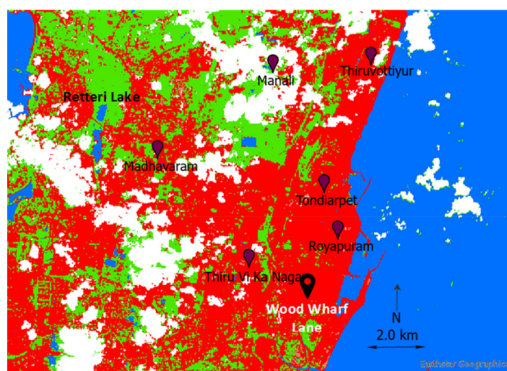
Pollution over the built areas is most pronounced between December and April before the scavenging action of the monsoon rain begins. This is observed in most Indian cities, which are heavily burdened with particulate matter, where pollution levels exceeding 1.5 times the pollution control board standards are observed (Ahuja, 2022).

The chosen study area for this study comprises the city of Madras, now known as Chennai, which is also a polluted Indian city (Figure 2a). This sprawling city's limits contribute to copious particulate emissions from

residential, industrial and transportation sources (Oanh et al., 2006; Prasannavenkatesh et al., 2015). The Southern and Western parts of Chennai constitute residential areas, whilst Central Chennai is mainly commercial. Whilst the upper and middle-class residential population typically uses liquefied petroleum gas (LPG) for domestic cooking, the lower-income group uses only kerosene, wood and other types of biofuels (Pavuluri et al., 2010), releasing particulates which mix freely with the city's aerosol cocktail comprising of sea salt (blown over from the adjoining Bay of Bengal) and ammonium sulphate (from DMS oxidation) present over most continental cities (Ghosh et al., 2018; Gumber et al., 2020; Gumber & Ghosh, 2022; Varun Raj et al., 2009). The aerosol particles caught in the convective updraughts; sometimes



(a)



(b)



(c)

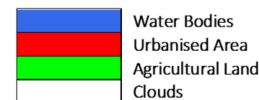


FIGURE 2 (a) Map of greater Chennai corporation limits-Central and North Chennai constitute higher slum population zones. The population density over the Central and North Chennai regions (marked in (a)), which includes Tondiarpet, Royapuram, Thiru.V. Ka Nagar, are respectively 563, 473 and 800 N/ha with very high number counts (Census of Tamilnadu, 2011). (b) Land use-land cover (LULC) variability in and around the North Chennai slums (b) during 2013 (c) during 2021. Note a 30% increase in the urbanized spaces around *Madhavaram* over a period of 8 years Source: GCC (2018)

cyclonic (Ghosh et al., 2014), serve as cloud condensation nuclei (CCN) which eventually grow into cloud droplets contributing to the city's cloud cover.

Nascent combustion-mediated particulate emissions, which are primarily hydrophobic, undergo a physico-chemical transformation in polluted environments rich in inorganic vapours enabling them to become hygroscopic (Lambe et al., 2011; Moteki et al. 2007; Petters et al., 2006; Shilling et al., 2007; Slade et al., 2015; Wong et al., 2011). A seminal study by Slade et al. (2015) conducted a flow-reactor analysis on the ageing of laboratory-generated biomass emissions exposed to hydroxyl ions (OH) and ozone (O₃) and also commented that lab studies on multiphase kinetics are scanty. In that study, the reactor conditions were maintained at standard pressure (1 atm) and temperature (25°C), and it was found that the hydrophobic particulates were rendered hydrophilic upon oxidation with OH. However, the lab conditions with regard to the uptake of such vapours did not conform to a 'real' atmosphere, where pressures and temperatures are orders of magnitude lower. In order to address this issue, in this study, parcel model simulations enabled the oxidation SO₂.H₂O in the presence of H₂O₂, O₃ as in the Slade et al. (2015) study, but over realistic pressure and temperature ranges.

Other studies have quantified the inorganic mass fraction of the processed hydrophilic substances within freshly emitted soot aggregates during biomass burning events (Schill et al., 2020; Yamasoe et al., 2000). Schill et al. (2020) undertook airborne missions to characterize biomass-mediated emissions over remote regions. The authors mention that global climate models are plagued with missing aerosol inventories of *fresh* and *aged* biomass emissions over remote stretches. The study found that due to the small size range of these emitted particles, they hover around for several days, enabling the accretion of soluble sulphate with median mass fractions between 0.2 and 0.6. In a similar vein, a recent study by Moteki et al. (2019) performed particle tracer analysis of *fresh* and *aged* black carbon particles and found that the hygroscopicity of black carbon emissions strongly modulated the scavenging efficiency impacting particle activation. However, these studies have not investigated how *aged* particles with varying quantities of surface deposits modulate the supersaturation field in a cloud parcel. With these observations, the existing research gaps that this present study will address are as follows:

1. To determine the extent of soluble sulphate accretion on the originally hydrophobic transient biomass mode through spectroscopic techniques and thence investigate thermodynamical and microphysical attributes of droplet growth in cloud parcels over the study region corresponding to a polluted urban area.

2. To relate the impact of the growth of cloud droplets over the polluted urban area on cloud cover over the city and to investigate conditions favouring rain suppression as well rain enhancements.

Since a multimodal aerosol spectrum comprising sea salt and ammonium sulphate over the region must also include transient emissions containing BC particles from the slums, it is essential to ascertain the spectral properties of these new emissions carefully. A combination of field studies, laboratory analysis, and microphysical aerosol-cloud modelling was undertaken to seek answers to the above questions. The scheme of the paper is as follows. In Section 2, we provide a survey of the North Chennai Slums, our study area. This is followed by a discussion on the experimental determination of the emission source strengths of biofuel stoves with the quantification of emissions. The chemical and microphysical analysis, including a morphological characterisation through a SEM analysis, is presented in Section 2.4.1. The aerosol size distribution is then determined, followed by the activation and growth of the spectrum in a cloud parcel (Section 3). The effects of the soluble mass fraction on the attenuation of the cloud parcel supersaturation profile are presented in Section 3, followed by implications of cook-stove generated particles on the cloud microphysics, including rain amount modulations from a large-eddy model. This is followed by conclusions and the wider implications discussed in Section 4.

2 | MATERIALS AND METHODS

2.1 | North Chennai slums – layout and land use and land cover (LULC) characterisation

The study zone comprising five major shantytown regions in Chennai, namely, *Madhavaram*, *Tondiarpet*, *Tiruvotiyur*, *Royapuram* and *Manali* (see Figure 2), have undergone rampant urbanisation mainly driven by increased migration from villages leading to an increase in population density (Philip, 2016). In this context, land use and land cover changes over a decadal time span enable a close quantification of the patterns of a changing urban landscape. LULC characterisation is performed over selected shantytown regions using Satellite-based Remote sensing procedures involving the use of Landsat-8 Operational Land Imager (OLI) images retrieved from the United States Geological Survey (USGS) (U.S. Geological Survey, 2013). LULC maps were developed from high-resolution (30 m spatial resolution) multispectral GeoTIFF images covering seven visible and near-infrared (VNIR) wavelength bands ranging between 0.43 and 2.29 μm using ArcGIS Pro (ESRI, 2021). The first step involved stacking of the

retrieved multi-spectral images to form a composite multi-band raster for subsequent downstream analysis. A supervised classification algorithm was used to obtain relevant training samples to classify images based on associated spectral signatures. Figure 2a,b shows the LULC maps over the study region for satellite passes spread over 8 years, that is, April 2013 and 2021, respectively.

One notices that over a period of 8 years, regions around *Madhavaram* (Zone III) and *Wood Wharf Lane* in *Royapuram* (Zone V) have undergone an unorganized urban expansion of up to 30% around an ecologically fragile wetland (Retteri lake). One also notices that the agricultural land around *Madhavaram* dwindled from 39% to 12% over this period. With a rapid increase in population density over this densely built-up area, there is a concomitant deterioration of air quality because the impoverished dwellers continue to use archaic cooking methods using solid cooking fuels (wood, dung cakes, etc.) (Gumber et al., 2020; Kumar et al., 2011). A site visit was necessary to determine the cooking practices, the type of stoves and biofuels used along with the exposure levels in and around the study region.

2.2 | Survey of slums over North Chennai

A door-to-door survey with a questionnaire revealed that the slum dwellers still use wood and cow dung cakes for preparing meals. A face-to-face meeting followed where the questionnaire (translated in the local vernacular, i.e., Tamil) was distributed to 50 slum households in Wood Wharf Lane (Zone V) where survey permission was granted (see Tables S1 and S2 in Data S1).

2.3 | Quantification of particulate matter from stove emissions

The exhaust emissions were passed through a constant volume sampler (Aerovironment-FPS 9000 High Volume Sampler, specifications: sampling rate up to 16.67 lpm

$\pm 10\%$) at a design flowrate of 1–1.25 lpm. The standard reference height for particle sampling was maintained at 3 m, and the instrument was placed at a distance of 2 m from emission sources as mandated by Tamil Nadu the Pollution Control Board. The instrument was carefully calibrated following the Orifice Transfer Standards, which involves measuring the pressure drop across the sampler orifice mounted firmly to the filter support. A calibration curve is then used to establish a relationship between the ascertained pressure difference and the associated flow rate (Kamyotra et al., 2012) (Figure 3).

The emanating particles (largely soot and black carbon) were collected onto pre-desiccated and pre-weighed glass-fibre filter papers ($20.3 \times 25.4 \text{ cm}^2$; Nupore-GF/1 model) firmly placed inside the sampling mount. After the completion of the experiment, the loosely lodged particles within the filter paper fibres were removed with a soft brush, and the filters were desiccated at 60°C overnight before undertaking a standard gravimetric analysis.

2.4 | Biomass emission characterisation

2.4.1 | SEM analysis of the particulate matter

The PM_{10} particles deposited onto the quartz filter paper in the high-volume sampler were analysed using scanning electron microscopy (SEM: electron gun with accelerating voltage 0.5–30 kV and Magnification range 5–8000 \times) (Figure 4).

To draw inferences on the atmospheric lifetimes of such transient emissions, it is essential to obtain the particle size distributions as well. A lognormal distribution was used to generate the particle size distribution (discussed in the next Section 3.1 under the sub-heading ‘Size Separation Analysis’), assuming a constant density of the deposited BC matter (1350 kg/m^3). A fuller procedure would involve Dynamic Light Scattering (DLS) characterisation of the collected particulates as discussed in Gumber and Ghosh (2022) and Gumber et al. (2022);



FIGURE 3 (a) High-volume sampler set up at a distance of 2 m upwind of the emission sources (b) same as (a) but standard reference height for particle sampling indicated

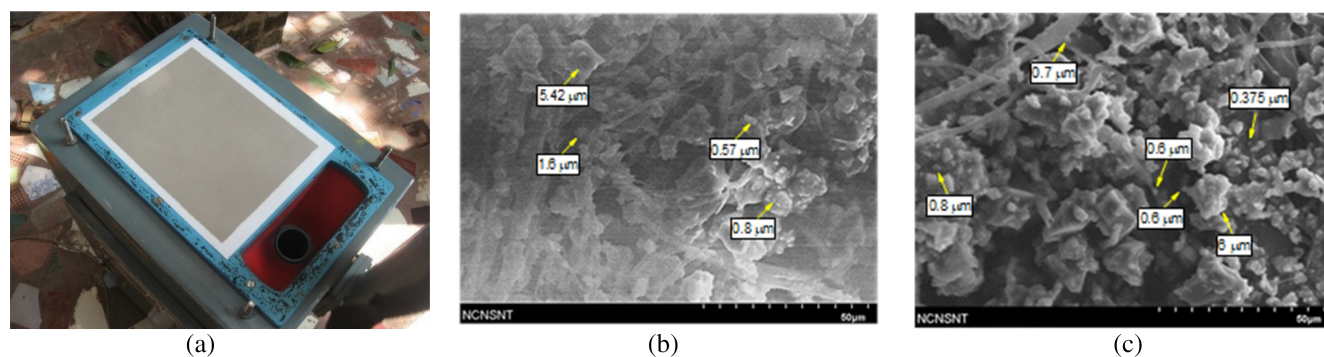


FIGURE 4 (a) PM_{10} particulate matter deposition causing a marked greying of the filter paper. (b) A SEM snapshot of PM_{10} emissions from cow dung combustion showing copious indentations. (c) SEM view of PM_{10} emissions from firewood combustion also showing copious surface indentations. Intricacies of the particle morphology were discernible at a magnification of $6000\times$. Images reveal the presence of numerous sub-micron radii particles distributed over the sampling location

TABLE 1 Sulphate concentrations obtained using a UV-spectrophotometer

Sample no.	Fuel	Average PM_{10} concentration at the highest flow rate ($mg\ m^{-3}$)	Iterations	Sulphates (SO_4^{2-}) in solution ($mg\ l^{-1}$)	Sulphates (SO_4^{2-}) per Vol of air ($mg\ m^{-3}$)	Soluble mass fraction (ϵ)
3	Cow dung	2173	1	720	381	
3	Cow dung		2	1010	534	
Average				865	458	0.21
6	Wood	2336	1	1800	952	
6	Wood		2	2000	1058	
Average				1900	1005	0.43

this was not possible because on-site particle analysers were not available with the Tamil Nadu Pollution Control Board. However, a Java-based image processing program, that is, ImageJ, is used for a preliminary size assessment of the collected particulates (ImageJ, 2011). This was sufficient for the primary estimation of SO_4^{2-} amounts accreted onto these particulates with varying radii.

2.5 | Compositional inferences of transient emissions from slum kitchens

Filter papers used in the high-volume sampler for PM_{10} particle collection were chemically analysed to detect water-soluble sulphate ions using UV spectrophotometry. The first step involved immersing a part of the filter paper in 20 ml of water for a period of 30 min. Thereafter, the collected soot particles were ultra-sonicated (Make: SONICS Vibra Cell) in double-distilled water at a fixed pulse duration of 30 s for a period of 10 min following established procedural norms (Gumber & Ghosh, 2022; Pecora, 2000). A sonication frequency of 20 kHz allowed for an efficient extraction of sulphate ions followed by

filtration of the extract through a 0.45-micron Whatman filter paper. Thereafter, the solution volume was made up to 25 ml for sulphate ion detection through a standard turbidity measurement (light absorbance at 420 nm on a UV-visible spectrophotometer) of the $BaSO_4$ suspension (Katz, 1977; Tanner & Newman, 1976). The concentration of sulphates per volume of air is shown in Table 1, and from these estimates, a crucial parameter-the soluble mass fraction calculated.

The soluble mass fraction estimated is 0.2–0.43 for this present set of experiments. It is interesting to compare the soluble mass fraction obtained from these urban slums with other measurements elsewhere. Comparable measurements over the Indian subcontinent were not reported; however, Yamasoe et al. (2000) made an estimate of this parameter for bioparticles released during forest fires in the Amazon area and found values ~ 0.25 . A seminal paper by Schill et al. (2020) reported sulphate mass fraction in biomass emissions between 0.2 and 0.6 during high biomass loading conditions.

Fresh biomass emissions coated with such hydrophilic materials can serve as cloud condensation nuclei (CCN) and can modulate the extent of cloud cover

TABLE 2 PM₁₀ mass concentration obtained from gravimetric analysis

Sample no.	Fuel	Mass of				Q_{avg} (l/min)	V (m ³)	PM ₁₀ (mg m ⁻³)	Emission rates (mg m ⁻³ s ⁻¹)
		M_i (g)	M_f (g)	PM_{10} (g)					
1	Cow dung	2.854	2.984	0.130	1	0.06	2173	0.604	
2	Cow dung	2.849	2.920	0.071	1	0.06	1184	0.328	
3	Cow dung	2.862	3.296	0.434	1.5	0.09	4819	1.338	
Average particle number count							7.5×10^6 particles cm ⁻³	Average: 0.756	
4	Wood	2.836	2.976	0.140	1	0.06	2336	0.648	
5	Wood	2.807	3.029	0.222	1	0.06	3686	1.023	
6	Wood	2.862	3.386	0.523	1.5	0.09	5822	1.617	
Average particle number count							10.9×10^6 particles cm ⁻³	Average: 1.096	

Note: Clearly, samples 3 and 6 correspond to the cases with the highest concentrations of PM₁₀ from cow dung and firewood, respectively. Average PM concentrations near the source from dung cake and fuelwood burning were 2725 mg/m³ and 3948 mg/m³, respectively. Additionally, PM₁₀ concentrations from fuelwood burning are higher by up to 40% when compared with emissions from dung cakes in consonance with past studies (Tiwari et al., 2014). The source strength far away was estimated to be $3 \times 10^{-6} \text{gs}^{-1} \text{m}^{-2}$, yielding a PM value of 200 $\mu\text{g}/\text{m}^3$.

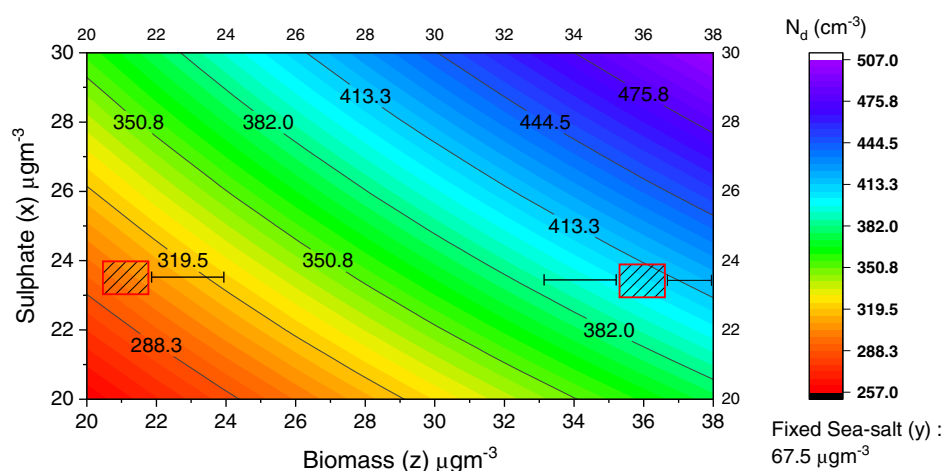


FIGURE 5 Cloud droplet counts (N_d) (numbers cm⁻³) as a function of sulphate and biomass concentrations ($\mu\text{g}/\text{m}^3$) predicted by the model runs. The activation process in the present case when specific sulphate, biomass smoke and sea-salt loadings are considered in the chemical parcel model (i.e., $10 \mu\text{g}/\text{m}^3$, $36 \mu\text{g}/\text{m}^3$ and $67.5 \mu\text{g}/\text{m}^3$, respectively and marked by a red rectangle positioned in the high biomass loading region) yields N_d value of ~ 415 droplets cm⁻³. Uncertainty in the modelled droplet count is around 8% arising from variabilities in the biomass mode numbers (Figure 7)

(Dusek et al., 2006; Gumber et al., 2022; Henning et al., 2010; Oshima et al., 2009). This is now explored.

2.6 | Subsequent microphysical implications

The growth of multiple aerosol modes (shown later in Figure 7) over Chennai was analysed first by using a Chemical Parcel Model (CPM). To explain the overall impact on the supersaturation profile due to varying chemical composition of the biomass emissions (the

effect of partial solubility), one must explore the growth profiles of individual modes.

2.6.1 | Overview of the chemical parcel model

A sophisticated Chemical Parcel Model (CPM) is used, which enables a bin-wise growth of dry aerosol particles into size-resolved cloud droplets (Ghosh et al., 2007; O'Dowd et al., 2000). The algorithm used within the model comprises of physics and chemistry modules. The

physics algorithm handles the cloud dynamical components and droplet growth, and the chemistry algorithm handles the gas/aqueous phase chemistry of aerosol particles coupled with non-ideal effects and distinguishes the types of the particles, in this instance, background sulphate and sea-salt particles, and transient biomass particles. The model is initialized with temperature, pressure, updraft speed and RH below the cloud base with respective values of 17.2°C, 877 mb, 1.0 ms⁻¹, 99.0% (<http://weather.uwyo.edu/upperair/sounding.html>).

2.6.2 | Transient biomass – characterisation in the chemical parcel model

Since the soluble mass on the aerosol particle modulates the overall density (ρ_t) of the particles concerned, an accurate apportioning of ρ_t is necessary (Ghosh et al., 2007; Gumber & Ghosh, 2022). Results from the parcel model simulations are shown for three levels of soluble sulphate content for the growth of transient biomass particles: 0.25 – the lower end of values observed, 0.5 – levels during a possible aggravated state, 0.75 – levels anticipated during the worst-case scenario (i.e., cases mediated by accidents). It is also important to investigate further the effect of these emissions on patterns of cloudiness over the study region. This is achieved by using WRF (Weather Research and Forecasting) model runs configured in the Large Eddy Model (LEM).

2.6.3 | Large Eddy simulation (LES)

To resolve the energy-containing eddies over the study region, that is, Chennai, the WRF model was configured in the large eddy model (Siebesma et al. 2003). The spatial resolution was maintained at 100 m in both the horizontal and vertical directions within a control volume of size 20 km × 20 km × 8 km. The model was configured with weather soundings, including potential temperature (θ), relative humidity, u and v winds (horizontal components of the wind vector) over *Chennai* for 15 December 2011 00:00:00 UTC (<http://weather.uwyo.edu/upperair/sounding.html>) when distinct cloud activity was observed. The choice of the simulation date coincides with the on-site experimentation time enabled by the PCB. Additionally, December falls within the Northeast monsoon season when one expects a significant cloud fraction. A spin-up time of 3 h was sufficient, and the results were analysed only during the final 3 h window with model outputs (3D) saved every 2 min.

A cloud microphysical scheme by Morrison et al. (2005) is used, which allows for double-moment warm as well as

cold cloud processes. However, configuring this scheme requires a prescription of cloud droplet number concentration which in turn depends on the aerosol count.

Several extant models rely on droplet activation routines mainly from a single component aerosol system, that is, ammonium sulphate, and thus are limited in their applicability to the wide variety of conditions which control droplet growth (Boucher & Lohmann, 1995; Jones et al., 1994; Menon et al., 2002; Quaas & Boucher, 2005). However, over polluted urban conurbations, biomass smoke is a recurring aerosol mode that mixes with other background modes (Gumber & Ghosh, 2022). Recent research over another polluted Indian city, that is, Hyderabad, suggested that biomass emissions undergo non-ideal heterogeneous sulphate accretion during repeated rounds of cloud processing such that the production of sulphate increases the water-soluble mass fraction of already existing biomass aerosols, making them even more hygroscopic (Gumber et al., 2022).

In this study, we estimate droplet counts from a tri-component aerosol system (experimentally derived transient biomass mode, background sulphate and sea salt modes) based on the procedures outlined by Rap et al. (2009). The authors show that for a tri-component system, the droplet numbers (N_d), although generally linearly depend on the aerosol numbers (N_a), can sometimes deviate from a linear dependence. In fact, they show that beyond a threshold, N_d versus N_a variation can be non-linear. We adopt the suggested method and show in Figure 5 that N_d versus N_a curves are only approximately linear but do not show plunging N_d values at high biomass loadings as in Rap et al. (2009).

To separate the perturbing effects of the transient emissions (from slums) from standard emissions, two cases are considered:

1. The ‘real’ case includes a cloud droplet count of 415 droplets cm⁻³ from all the aerosol modes shown in Figures 5 and 7.
2. The ‘baseline’ case with reduced transient emissions and a 27% lower N_d of 300 droplets cm⁻³ (Figure 5).

In the next section, we discuss the consequent experimental and modelling results.

3 | RESULTS AND DISCUSSIONS

3.1 | Aerosol spectra characterisation of slum emissions

It is essential first to ascertain the presence of distinct categories of aerosols. Chennai’s presence along the Bay of

Bengal has sea salt mixed with ammonium sulphate (sourced from DMS oxidation) in its boundary layer. Whilst these two types are expected to be ubiquitously present (Gumber et al., 2020; Kommula et al., 2021), it is also important to detect aerosol signatures from more localized anthropogenic sources. With this background information, a reasonable starting point should relate to ‘Satellite-based Aerosol Characterisation’.

3.1.1 | Satellite-based aerosol characterisation

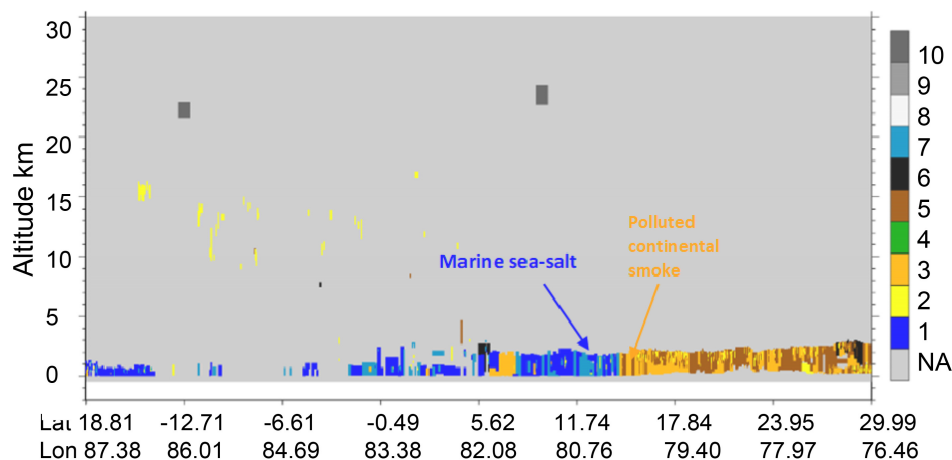
Aerosol signatures over the region were identified based on the satellite transects of aerosol layers retrieved from the CALIPSO Version 4.1 LIDAR dataset (Young &

Vaughan, 2009; Anselmo, 2006; Hogan, 2006) (http://www.calipso.larc.nasa.gov/products/CALIPSO_DPC_Rev2x4.pdf) (see S2). The day and night-time observations (Figure 6a,b) show continental smoke as well as marine particles covering the entire boundary layer up to 2.5 km during December 2011.

Thus, Figure 6a,b shows the unmistakable presence of black carbon smoke within Chennai City and call for a fuller investigation.

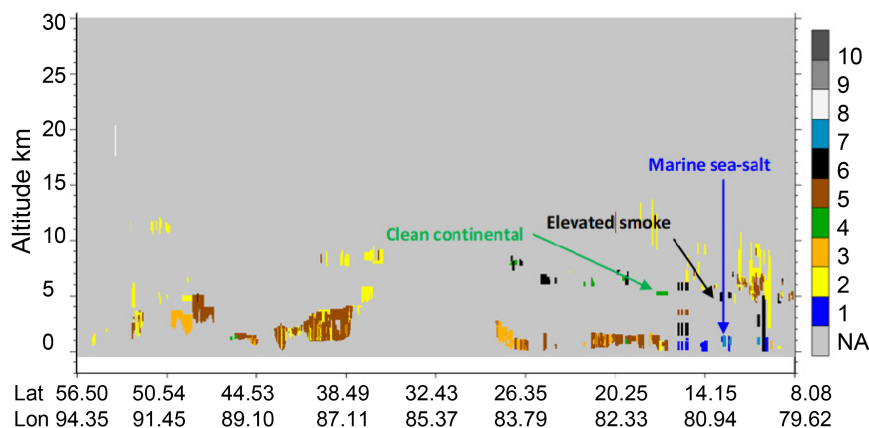
3.1.2 | Gravimetric analysis of emissions from slum-kitchens

In Table 2, gravimetric measurements of the deposited particulates from fuelwood and dung cake emissions



N/A = not applicable; 1 = marine; 2 = dust; 3 = polluted continental/smoke; 4 = clean continental; 5 = polluted dust; 6 = elevated smoke; 7 = dusty marine; 8 = PSC aerosol; 9 = volcanic ash; 10 = sulphate/others

(a)



N/A = not applicable; 1 = marine; 2 = dust; 3 = polluted continental/smoke; 4 = clean continental; 5 = polluted dust; 6 = elevated smoke; 7 = dusty marine; 8 = PSC aerosol; 9 = volcanic ash; 10 = sulphate/others

(b)

FIGURE 6 (a) Day-time observation of aerosol sub-types from LIDAR observations from a satellite pass in December 2011 showing the presence of continental and marine particles over the region of interest. (b) Night-time observation also shows the presence of smoke

along with their PM concentrations recorded by the high-volume sampler are tabulated.

Although the preceding gravimetric analysis detailed in Table 2 shows the variability of mass amounts collected from the two fuel types, that is, cow-dung and fuel-wood, this information must be supplanted with procedures related to a size-segregated apportioning. The latter is vital for a deeper understanding of which particle modes are able to impact the supersaturation profiles more profoundly. Specific size ranges are more prone to continuous growth (starting from the parcel's base and reaching up to the cloud top) than others. When this study was undertaken in 2011, facilities such as Scanning Mobility Particle Analysers (SMPS) and Differential Mobility Analysers (DMA) were unavailable with the Pollution Control Board. However, the overseeing government organisation, that is, Tamil Nadu Pollution Control Board, had some suggested guidelines, which included a SEM analysis of the collected material following earlier studies (Dominko et al., 2003).

3.1.3 | Size separation analysis

Figure 4 shows the presence of size variegated particles within a radii range 0.1–10 μm . The SEM imagery was imported into an imaging software, Image J, to ascertain the dominant modal radius by ascribing colour thresholds (in this instance, varying shades of grey) to isolate individual particles (Kumal et al., 2020)- the modal radius for cow-dung and fuelwood mediated particulates was determined to be 0.4 μm . Having established the modal size, it becomes imperative to ascribe realistic numbers to specific size classes. This was challenging because particle counting at the source was not an option then. However, studies, including the works of Tiwari et al. (2014) and Johansson et al. (2003), established that the modal radii were sub-micron, so the assumption of sphericity was invoked. There are known deviations from sphericity at larger sizes (Nakagawa et al., 2020). With an assumption of 1350 $\text{kg}\cdot\text{m}^{-3}$ as the density of black carbon, along with the assumption of entirely spherical particles, it was straightforward to gauge the particle number densities.

3.1.4 | Ascertaining overall aerosol signatures over study region

PM_{10} concentrations (m) sourced from the high-volume sampler readings (Table 2) combined with the modal size (r_m) ascertained from the above procedure yielded the corresponding particle numbers $N = (3m)/(4\pi\rho r^3)$ to be $7.5 \times \text{particles cm}^{-3}$ and $10.9 \times \text{particles cm}^{-3}$ for cow

and wood, respectively, consonant with other established procedures involving an SMPS (Johansson et al., 2003; Tiwari et al., 2014). The last step involved plotting a lognormal distribution with the known values of N , r_m and σ (Standard spectral spread; Ghosh et al., 2007) as shown in Figure 7. Since the PSD's have similar spectral spreads, an average log-normal distribution is used for subsequent modelling analysis. These distributions (red and violet line plots in Figure 7) reveal that the proportion of sub-micron sized particles is predominant in the entire spectrum of particles emitted during the experiment. Figure 7 shows how the transient modes compare with other dominant aerosol spectra over the city, that is, $(\text{NH}_4)_2\text{SO}_4$ and NaCl.

The modal variabilities in the error bars for cow dung and fuel wood emissions are ± 30 particles and ± 36.89 particles, respectively (see Figure 7).

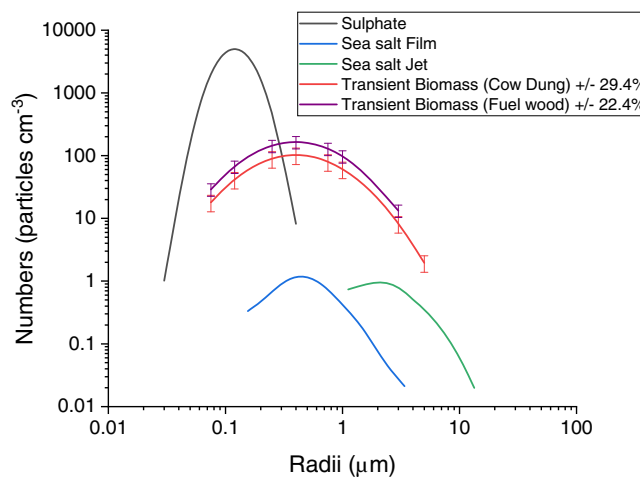


FIGURE 7 Dry aerosol spectra for all four modes: sea salt-jet & film modes, sulphate mode, biomass-transient mode determined experimentally. The global sulphate mode peaks at the smallest size of 0.12 μm radius. Additionally, the film mode salt particles and transient biomass particles from cookstoves are also within the accumulation mode regime. The standard deviations in the spectra are obtained from Ghosh et al. (2007). Interestingly, the transient biomass loading covers the broadest range of aerosol particles of size 0.1 to 10 μm in agreement with other studies (Gumber et al., 2022; Gumber & Ghosh, 2022). Note the associated uncertainties in the number counts of transient biomass modes represented through error bars. Modal variability in the error bars is ± 30 particles cm^{-3} and ± 36.89 particles cm^{-3} for cow dung and fuel wood, respectively. In order to obtain the particle concentrations above the surface layer (100 m vertically upwards) and around the slum clusters during December 2011, a Gaussian Plume model (AERMOD) was used, which accounted for the advective and diffusive processes as these particles ascend, yielding an average particle count of $\sim 110 \pm 36.89$ particles cm^{-3} (σ_y : 31.4 m and σ_z : 25.17 m for a downwind distance of 100 m) (Gumber et al., 2022; Perry et al., 2005)

3.2 | Effect of soluble mass fraction of the accreted sulphate (ϵ) on the Supersaturation and droplet growth profiles for transient biomass mode

Figure 8a shows the supersaturation profiles, respectively, for varying soluble mass fraction (ϵ) value of the accreted sulphate between 0.25 and 0.75, at a moderate updraught speed of 1.0 m/s. It is observed that the maximum supersaturation approaches 0.026% when ϵ is 0.25.

Some of the transient particles are able to grow to droplet radii of the order of 35 μm (largest biomass bin shown in Figure 8b) at the expense of other fully soluble aerosol particles. At these sizes, they have already exceeded the critical threshold radii of 20 μm , kick-starting a collision-coalescence process (Ghosh et al., 2005) – they capture not only the smaller biomass particle mediated drops but all the other cloud droplets generated from other modes. This is possibly the main reason why researchers have found that urban emissions can well affect cloud activity (Guo et al., 2019). Unlike the other modes, these biomass emissions are present in overwhelming numbers and are dependent on the fuel type (Haynes & Wagner, 1981; Rehman et al., 2011; Tiwari et al., 2014).

In the next section, we investigate the impact of such aerosol loadings on local cloud morphology when they

are included within a bulk hydrometeor scheme in the Weather Research and Forecasting (WRF) model.

3.3 | Implications of cook-stove generated particles on boundary layer processes from a large-eddy model

3.3.1 | Effects on cloud cover and rain amount

Figure 9c,e shows the morphological organisation of the cloud where the droplet numbers generated from the procedures outlined in Section 2.6.2 are included in the cloud microphysical scheme. One observes the geometrical thickness of the cloud to be 2500 m, with the cloud base and top at 1.5 km and ~ 4 km, respectively.

The Mean cloud optical depth (54) in the ‘real’ case compares well with the observed range of τ , varying between 45 and 55 for this day (Product: MODIS – Terra MOD08_D3 v6.1) (Figure 9a; Table 3). A higher number of cloud droplets in the ‘real’ case (~ 415 droplets cm^{-3}) yields a higher cloud coverage of 56% (Figure 9c,e) in agreement with earlier studies (Lee, 2011; Storer & van den Heever, 2013). The baseline rain rates show large deviations from observations beyond 5 h; neither does it capture the peak earlier on at 4.5 h (Figure 9b). Table 3

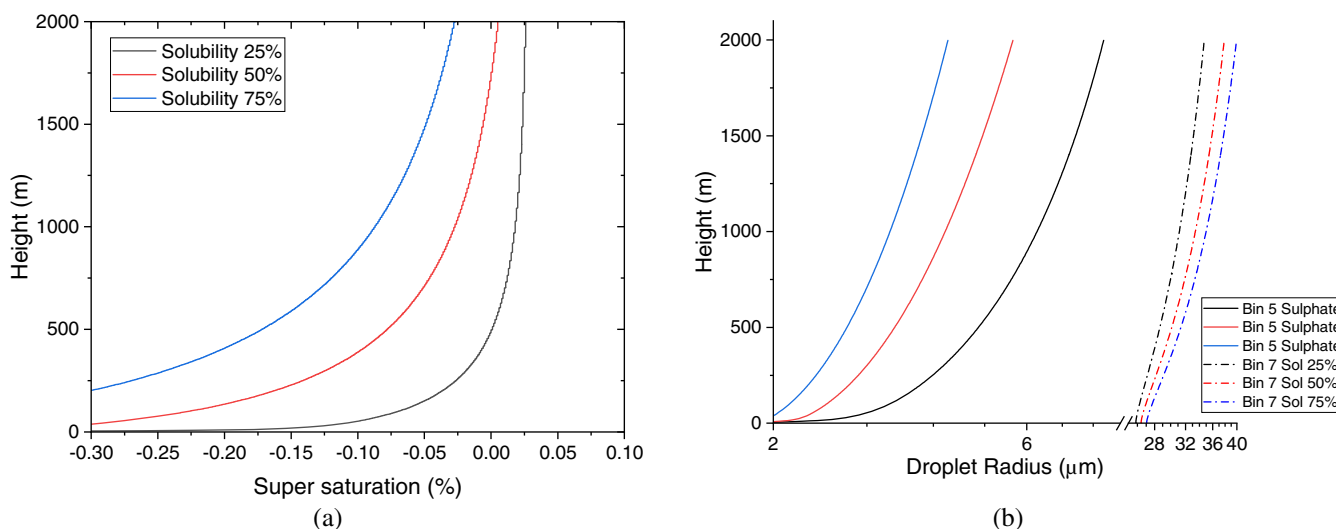


FIGURE 8 (a) Supersaturation versus height profile variation with varying soluble mass fraction value (ϵ) of the transient mode. The supersaturation value falls with increasing fractional solubility of the accreted sulphate amounts demonstrating the attenuating effect of soluble matter on the supersaturation profiles. When more soluble matter is present within the fine indentations of the transient mode, a greater number of particles compete for the available moisture, thereby lowering the maximum supersaturation even at a modest updraught speed of 1 m/s. (b) Droplet growth profiles for sulphate and biomass modes at varying soluble mass fractions of the accreted sulphate only on the biomass mode. Note the increased growth rates for the transient black carbon-based droplets with higher soluble mass fractions of the accreted sulphate. A lower water vapour saturation value attained in the ‘high solubility’ case impedes the growth of fully soluble sulphate-based cloud droplets, which are the most numerous (solid blue line in (b))

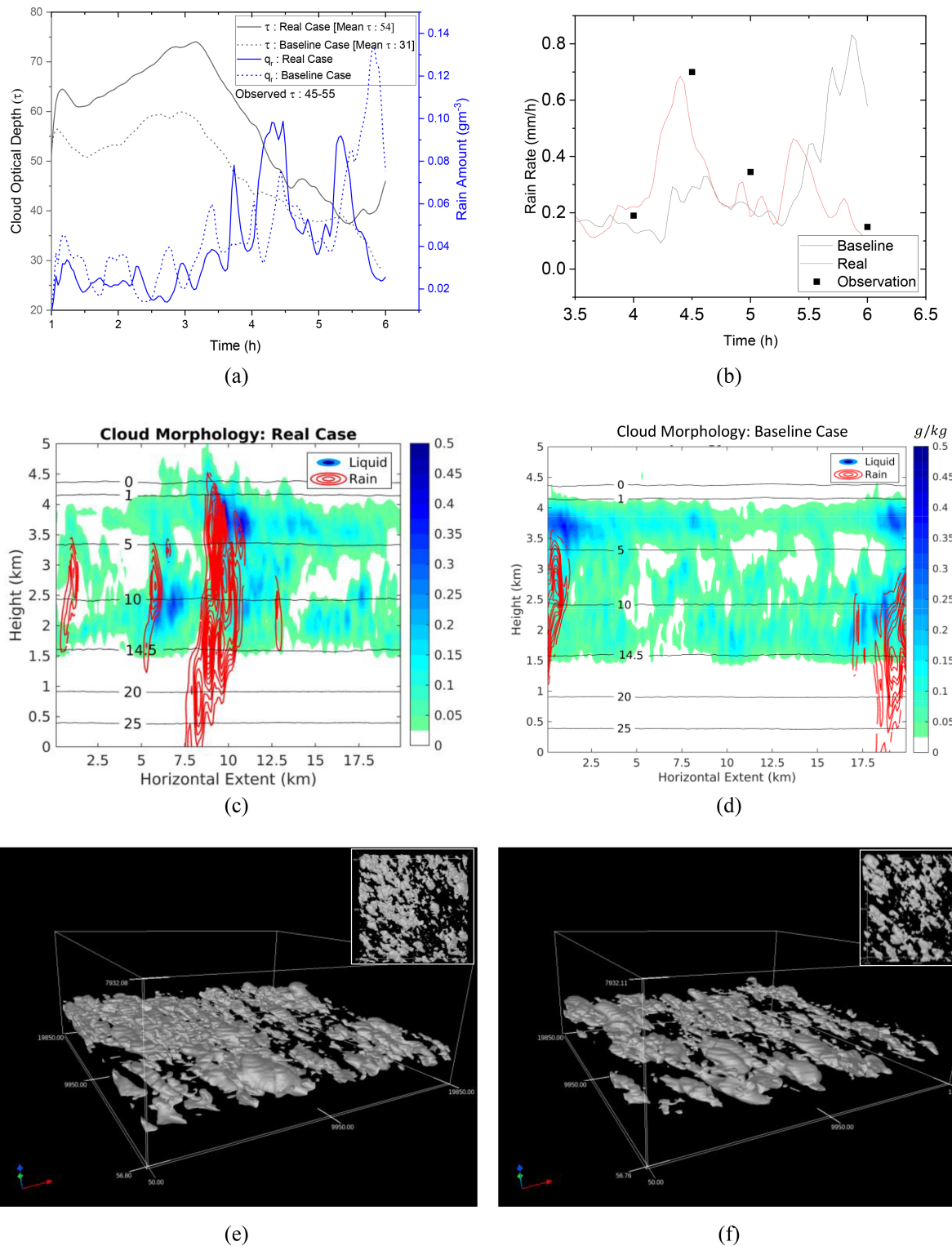


FIGURE 9 (a) Time evolution of cloud optical depths and rainwater amounts for the two cases, that is, the real case and the baseline case. An episode of intense downpour in the real case post 3.5 h follows from an initial phase of warm-rain suppression (b) modelled and observed drizzle rates for the two cases over the study region (observation: global precipitation mission's IMERG dataset GPM_3IMERGHH_V06, domain: 79.541°E, 12.5732°N, 80.1563°E, 13.2763°N). (c) Modelled cloud and rain amount time-averaged over a 30 min period during stable cloud growth conditions for the 'real' case (d) same as (c) but for the 'baseline case'. (e) 3D iso-surface of cloud water amount for the 'real' case generated using VAPOR (f) same as (e) but for the 'baseline' case. Note the increased levels of cloud cover in the 'real' case

TABLE 3 A comparison of modelled ('real' case) versus observational variables

Variable	Modelled (real case)	Observed
Cloud optical depth	54	45–55
Cloud-top altitude	~4.5–5 km (535 – 575 hPa)	~4.8–5.2 km (525 – 550 hPa)
Cloud-base altitude	1.45 km	1.0–1.5 km
Cloud-deck thickness	3–3.6 km	3.3–4.2 km

Note: Data source: Cloud optical depth and cloud top pressure (hPa) – MODIS atmosphere L3 monthly product (08_L3) (Platnick et al., 2015). NASA MODIS adaptive processing system, Goddard Space Flight Center. https://doi.org/10.5067/MODIS/MYD08_M3.006 (Terra); GMAO (2015), cloud base altitude determined from the vertical profile of 3-hourly averaged cloud fraction (MERRA-2 pressure-level, assimilation, radiation diagnostics V5.12.4 (M2T3NPRAD)); (region domain: 79.5°E, 12.57°N, 80.15°E, 13.27°N).

shows a comparison between the modelled and observed variables. It is very clear from Table 3 that model results agree remarkably well with the observed values.

4 | CONCLUSIONS AND WIDER IMPLICATIONS

This first study shows through carefully constructed experimental and modelling analyses that over large urban conurbations, biomass emissions emanating from shantytown settlements significantly modulate the local cloud microphysics. A UV-spectroscopy analysis revealed that the morphological indentations within the observed size segregated stove emissions contained soluble sulphates with mass fractions between 0.2 and 0.43 rendering these particles partially soluble in conformation with past studies. When such particles are included within a sophisticated chemical parcel model, they activate and grow into full-fledged cloud droplets even at modest values of the updraught speeds. This study also illustrates for the first time the attenuating effect of the accreted sulphate on the parcel's super-saturation profile. Moreover, when such local emissions are incorporated within a large-scale model, increased cloudiness by up to 25% is noted, and modelled cloud optical depths also agree better with observations. The study also indicates an increase in condensate loading within a deeper cloud only when the droplet contribution from the 'transient mode' comprising of slum emissions is included with the ensuing drizzle rates also agreeing favourably with observations. Also, an episode of intense downpour follows from an initial phase of warm-rain suppression. These densely packed settlements built up with flimsy building

materials experience heavy downpour routinely with a loss of livelihood. Such localized microphysical alterations affecting cloud cover and precipitation amounts should feature in urban planning models over South Asian cities.

AUTHOR CONTRIBUTIONS

Sathish Chellaiah: Data curation; investigation; methodology; writing – review and editing. **Siddharth Gumber:** Methodology; software; visualization; writing – review and editing. **Steve Dobbie:** Formal analysis; methodology; writing – review and editing. **Huiyi Yang:** Formal analysis; methodology; writing – review and editing.

ACKNOWLEDGEMENT

The authors would like to acknowledge High Speed Computing facilities under the ERASMUS+ Capacity Building Scheme for Higher Education.

FUNDING INFORMATION

This research received no external funding.

CONFLICT OF INTEREST

The authors declare that there are no conflicts of interest.

DATA AVAILABILITY STATEMENT

Not applicable.

ORCID

Satyajit Ghosh  <https://orcid.org/0000-0002-1643-006X>

Siddharth Gumber  <https://orcid.org/0000-0002-1648-1537>

REFERENCES

- Ahuja, A. (2022) World air quality report 2021: 63 Indian cities in 100 most polluted places on earth. *NDTV-Dettol Banega Swasth Swachh India*. Available at: <https://swachhindia.ndtv.com/world-air-quality-report-2021-63-indian-cities-in-100-most-polluted-places-on-earth-67358/> [Accessed 5th April 2022].
- Anselmo, T. (2006) *Cloud-aerosol LIDAR infrared pathfinder satellite observations: data management system, data products catalog*. Document No: PC-SCI-503. Hampton, VA. Available at: NASA, Langley Research Center. http://www-calipso.larc.nasa.gov/products/CALIPSO_DPC_Rev2x4.pdf
- Boucher, O. & Lohmann, U. (1995) The sulphate-CCN-cloud albedo effect—a sensitivity study with two general circulation models. *Tellus*, 47B, 281–300.
- Census of Tamilnadu. (2011) *Chennai, village and town directory*. Tamil Nadu, India: Directorate of Census Operations, p. 241.
- Ding, K., Huang, X., Ding, A., Wang, M., Su, H., Kerminen, V.M. et al. (2021) Aerosol-boundary-layer-monsoon interactions amplify semi-direct effect of biomass smoke on low cloud formation in Southeast Asia. *Nature Communications*, 12, 6416. <https://doi.org/10.1038/s41467-021-26728-4>

- Dominko, R., Gaberscek, M., Drogenik, J., Bele, M., Pejovnik, S. & Jamnik, J. (2003) The role of carbon black distribution in cathodes for Li ion batteries. *Journal of Power Sources*, 119–121, 770–773. [https://doi.org/10.1016/S0378-7753\(03\)00250-7](https://doi.org/10.1016/S0378-7753(03)00250-7)
- Dusek, U., Reischl, G.P. & Hitznerberger, R. (2006) CCN activation of pure and coated carbon black particles. *Environmental Science & Technology*, 40, 1223–1230. <https://doi.org/10.1021/es0503478>
- ESRI. (2021) *ArcGIS*. Redlands, CA: Environmental Systems Research Institute.
- GCC. (2018) *Zone details, greater Chennai corporation*. Available at: <http://chennaicorporation.gov.in/zone/index.htm>
- Ghanti, R. & Ghosh, S. (2010) The great Indian haze revisited: aerosol distribution effects on microphysical and optical properties of warm clouds over peninsular India. *Advances in geosciences*, 25, 51–54. <https://doi.org/10.5194/adgeo-25-51-2010>
- Ghosh, S., Dávila, J., Hunt, J.C.R., Srdic, A., Fernando, H.J.S. & Jonas, P.R. (2005) How turbulence enhances coalescence of settling particles with applications to rain in clouds. *Proceedings of the Royal Society A*, 461, 3059–3088. <https://doi.org/10.1098/rspa.2005.1490>
- Ghosh, S., Gumber, S. & Varotsos, C. (2018) A sensitivity study of diffusional mass transfer of gases in tropical storm hydrometeors. *Theoretical and Applied Climatology*, 134(3–4), 1083–1100. <https://doi.org/10.1007/s00704-017-2321-4>
- Ghosh, S., Smith, M.H. & Rap, A. (2007) Integrating biomass, sulphate and sea-salt aerosol responses into a microphysical chemical parcel model: implications for climate studies. *Philosophical Transactions of the Royal Society A: Mathematical, Physical and Engineering Sciences*, 365(1860), 2659–2674. <https://doi.org/10.1098/rsta.2007.2082>
- Ghosh, S., Vidyasagan, V. & Sandeep, S. (2014) Smart cyclone alerts over the Indian subcontinent. *Atmospheric Science Letters*, 15, 157–158. <https://doi.org/10.1002/asl2.486>
- Global Modeling and Assimilation Office (GMAO). (2015) *MERRA-2 tavg3_3d_rad_Np: 3d,3-Hourly,Time-Averaged,Pressure-Level,Assimilation,Radiation Diagnostics V5.12.4*. Greenbelt, MD: Goddard Earth Sciences Data and Information Services Center (GES DISC), [Accessed 3rd June 2022]. <https://doi.org/10.5067/3UGE8WQXZAK>
- Gumber, S. & Ghosh, S. (2022) An experimental and modelling analysis of cloud droplet growth from vehicular emissions with non-ideal microphysics over an Asian mega-city. *Atmospheric Science Letters*, 23, e1081. <https://doi.org/10.1002/asl.1081>
- Gumber, S., Ghosh, S., Bera, S. & Prabhakaran, T.V. (2022) On the importance of non-ideal sulphate processing of multi-component aerosol haze over urban areas. *Meteorology and Atmospheric Physics*, 134, 37. <https://doi.org/10.1007/s00703-022-00877-7>
- Gumber, S., Ghosh, S., Orr, A., Sathish Kumar, C.R. & Pope, J. (2020) On the microphysical processing of aged combustion aerosols impacting warm rain microphysics over Asian megacities. *Theoretical and Applied Climatology*, 139, 1479–1491. <https://doi.org/10.1007/s00704-019-03042-0>
- Guo, J., Li, Y., Cohen, J.B., Li, J., Chen, D., Hui, X. et al. (2019) Shift in the temporal trend of boundary layer height in China using long-term (1979–2016) radiosonde data. *Geophysical Research Letters*, 46(11), 6080–6089. <https://doi.org/10.1029/2019GL082666>
- Guttikunda, S.K. & Kopakka, R.V. (2014) Source emissions and health impacts of urban air pollution in Hyderabad, India. *Air Quality, Atmosphere and Health*, 7, 195–207.
- Haynes, B.S. & Wagner, H.G. (1981) Soot formation. *Progress in Energy and Combustion Science*, 7, 229–273. [https://doi.org/10.1016/0360-1285\(81\)90001-0](https://doi.org/10.1016/0360-1285(81)90001-0)
- Henning, S., Wex, H., Hennig, T., Kiselev, A., Snider, J.R., Rose, D. et al. (2010) Soluble mass, hygroscopic growth, and droplet activation of coated soot particles during LACIS Experiment in November (LExNo). *Journal of Geophysical Research: Atmospheres*, 115, D11206. <https://doi.org/10.1029/2009JD012626>
- Hogan, R.J. (2006) Fast approximate calculation of multiply scattered lidar returns. *Applied Optics*, 45, 5984–5992. <https://doi.org/10.1364/AO.45.005984>
- ImageJ. (2011) *Research services branch*. Bethesda, MD. Available at: National Institute of Mental Health. <https://imagej.nih.gov/ij/>
- Johansson, L.S., Tullin, C., Leckner, B. & Sjövall, P. (2003) Particle emissions from biomass combustion in small combustors. *Biomass and Bioenergy*, 25, 435–446. [https://doi.org/10.1016/S0961-9534\(03\)00036-9](https://doi.org/10.1016/S0961-9534(03)00036-9)
- Jones, A., Roberts, D.L. & Slingo, A. (1994) A climate model study of indirect radiative forcing by anthropogenic sulphate aerosols. *Nature*, 370, 450–453. <https://doi.org/10.1038/370450a0>
- Kamyotra, J.S., Saha, D., Tyagi, S.K. et al. (2012) *Guidelines for manual sampling & analyses*. Parivesh Bhawan, East Arjun Nagar, Delhi: Central Pollution Control Board.
- Katz, M. (1977) *Methods of air sampling and analysis*. Washington, DC: American Public Health Association.
- Kommula, S.M., Upasana, P., Sharma, A., Raj, S.S., Reyes-villegas, E., Liu, T. et al. (2021) Chemical characterization and source apportionment of organic aerosols in the Coastal City of Chennai, India: impact of marine air masses on aerosol chemical composition and potential for secondary organic aerosol formation. *ACS Earth and Space Chemistry*, 5, 3197–3209. <https://doi.org/10.1021/acsearthspacechem.1c00276>
- Kumal, R.R., Liu, J., Gharpure, A., Vander Wal, R.L., Kinsey, J.S., Giannelli, B. et al. (2020) Impact of biofuel blends on black carbon emissions from a gas turbine engine. *Energy & Fuels*, 34, 4958–4966. <https://doi.org/10.1021/acs.energyfuels.0c00094>
- Kumar, C.R.S., Ghosh, S., Sethia, K. & Picardo, J. (2011) Bioparticle emission and distribution over slums in a tropical India metropolis. Poster presented at the *European aerosol conference*, Manchester, UK.
- Lambe, A.T., Onasch, T.B., Massoli, P., Croasdale, D.R., Wright, J. P., Ahern, A.T. et al. (2011) Laboratory studies of the chemical composition and cloud condensation nuclei (CCN) activity of secondary organic aerosol (SOA) and oxidized primary organic aerosol (OPOA). *Atmospheric Chemistry and Physics*, 11, 8913–8928. <https://doi.org/10.5194/acp-11-8913-2011>
- Lee, S.S. (2011) Dependence of aerosol-precipitation interactions on humidity in a multiple-cloud system. *Atmospheric Chemistry and Physics*, 11, 2179–2196. <https://doi.org/10.5194/acp-11-2179-2011>
- Menon, S., Del Genio, A.D., Koch, D. & Tselioudis, G. (2002) GCM simulations of the aerosol indirect effect: sensitivity to cloud parameterisation and aerosol burden. *Journal of the Atmospheric Sciences*, 59, 692–713.
- Morrison, H., Curry, J.A. & Khvorostyanov, V.I. (2005) A new double-moment microphysics parameterization for application

- in cloud and climate models. Part I: Description. *Journal of the Atmospheric Sciences*, 62, 1665–1677. <https://doi.org/10.1175/JAS3446.1>
- Moteki, N., Kondo, Y., Miyazaki, Y., Takegawa, N., Komazaki, Y., Kurata, G. et al. (2007) Evolution of mixing state of black carbon particles: aircraft measurements over the western Pacific in March 2004. *Geophysical Research Letters*, 34, L11803. <https://doi.org/10.1029/2006GL028943>
- Moteki, N., Mori, T., Matsui, H. & Ohata, S. (2019) Observational constraint of in-cloud supersaturation for simulations of aerosol rainout in atmospheric models. *NPJ Climate and Atmospheric Science*, 2, 1–11. <https://doi.org/10.1038/s41612-019-0063-y>
- Nakagawa, M., Nakayama, T., Sasago, H., Kuruma, Y., Yai, H., Ogawa, S. et al. (2020) Assessment of the sphericity of submicrometer particles using a single-particle polar nephelometer at an urban site in Japan. *Aerosol and Air Quality Research*, 20, 2474–2484. <https://doi.org/10.4209/aaqr.2020.01.0023>
- Oanh, N.T.K., Upadhyay, N., Zhuang, Y.-H., Hao, Z.P., Murthy, D. V.S., Lestari, P. et al. (2006) Particulate air pollution in six Asian cities: spatial and temporal distributions, and associated sources. *Atmospheric Environment*, 40, 3367–3380. <https://doi.org/10.1016/j.atmosenv.2006.01.050>
- O'Dowd, C.D., Lowe, J.A., Clegg, N. et al. (2000) Modeling heterogeneous sulphate production in maritime stratiform clouds. *Journal of Geophysical Research: Atmospheres*, 105, 7143–7160. <https://doi.org/10.1029/1999JD900915>
- Oshima, N., Koike, M., Zhang, Y., Kondo, Y., Moteki, N., Takegawa, N. et al. (2009) Aging of black carbon in outflow from anthropogenic sources using a mixing state resolved model: model development and evaluation. *Journal of Geophysical Research: Atmospheres*, 114, D06210. <https://doi.org/10.1029/2008JD010680>
- Padmakumari, B., Maheskumar, R.S., Harikishan, G., Morwal, S.B., Prabha, T.V. & Kulkarni, J.R. (2013) In situ measurements of aerosol vertical and spatial distributions over continental India during the major drought year 2009. *Atmospheric Environment*, 80, 107–121. <https://doi.org/10.1016/j.atmosenv.2013.07.064>
- Pavuluri, C.M., Kawamura, K., Tachibana, E. & Swaminathan, T. (2010) Elevated nitrogen isotope ratios of tropical Indian aerosols from Chennai: implication for the origins of aerosol nitrogen in South and Southeast Asia. *Atmospheric Environment*, 44, 3597–3604. <https://doi.org/10.1016/j.atmosenv.2010.05.039>
- Pecora, R. (2000) Dynamic Light Scattering Measurement of Nanometer Particles in Liquids. *Journal of Nanoparticle Research*, 2, 123–131.
- Perry, S.G., Cimarelli, A.J., Weil, J.C., Venkatram, A., Paine, R.J., Wilson, R.B. et al. (2005) AERMOD: a dispersion model for industrial source applications. Part II: Model performance against seventeen field-study databases. *Journal of Applied Meteorology*, 44, 694–708.
- Petters, M.D., Prenni, A.J., Kreidenweis, S.M., DeMott, P.J., Matsunaga, A., Lim, Y.B. et al. (2006) Chemical aging and the hydrophobic-to-hydrophilic conversion of carbonaceous aerosol. *Geophysical Research Letters*, 33, L24806. <https://doi.org/10.1029/2006GL027249>
- Philip, C.M. (2016) *Slums in Chennai increase by 50% in a single decade*. The Times of India. Available at: <https://timesofindia.indiatimes.com/city/chennai/slums-in-chennai-increase-by-50-in-a-single-decade/articleshow/50618951.cms> [Accessed 30th March 2022].
- Platnick, S., Hubanks, P., Meyer, K. & King, M.D. (2015) MODIS atmosphere L3 monthly product (08_L3). NASA MODIS Adaptive Processing System, Goddard Space Flight Center. https://doi.org/10.5067/MODIS/MYD08_M3.006
- Prasannavenkatesh, R., Andimuthu, R., Kandasamy, P., Rajadurai, G., Kumar, D.S., Radhapriya, P. et al. (2015) Assessment of population exposure to coarse and fine particulate matter in the urban areas of Chennai, India. *The Scientific World Journal*, 2015, e643714. <https://doi.org/10.1155/2015/643714>
- Quaas, J. & Boucher, O. (2005) Constraining the first aerosol indirect radiative forcing in the LMDZ GCM using POLDER and MODIS satellite data. *Geophysical Research Letters*, 32, L17814. <https://doi.org/10.1029/2005GL023850>
- Rap, A., Ghosh, S. & Smith, M.H. (2009) Shepard and hardy multi-quadratic interpolation methods for multicomponent aerosol-cloud parameterization. *Journal of the Atmospheric Sciences*, 66, 105–115. <https://doi.org/10.1175/2008JAS2626.1>
- Rehman, I.H., Ahmed, T., Praveen, P.S., Kar, A. & Ramanathan, V. (2011) Black carbon emissions from biomass and fossil fuels in rural India. *Atmospheric Chemistry and Physics*, 11, 7289–7299. <https://doi.org/10.5194/acp-11-7289-2011>
- Schill, G.P., Froyd, K.D., Bian, H., Kupc, A., Williamson, C., Brock, C.A. et al. (2020) Widespread biomass burning smoke throughout the remote troposphere. *Nature Geoscience*, 13, 422–427. <https://doi.org/10.1038/s41561-020-0586-1>
- Sharma, A.R., Kharol, S.K. & Badarinath, K.V.S. (2010) Influence of vehicular traffic on urban air quality – a case study of Hyderabad, India. *Transportation Research Part D: Transport and Environment*, 15, 154–159.
- Shilling, J.E., King, S.M., Mochida, M., Worsnop, D.R. & Martin, S. T. (2007) Mass spectral evidence that small changes in composition caused by oxidative aging processes alter aerosol CCN properties. *The Journal of Physical Chemistry. A*, 111, 3358–3368. <https://doi.org/10.1021/jp068822r>
- Siebesma, A.P., Bretherton, C.S., Brown, A., Chlond, A., Cuxart, J., Duynkerke, P.G. et al. (2003) A large Eddy simulation inter-comparison study of shallow cumulus convection. *Journal of the Atmospheric Sciences*, 60, 1201–1219. [https://doi.org/10.1175/1520-0469\(2003\)60<1201:ALESIS>2.0.CO;2](https://doi.org/10.1175/1520-0469(2003)60<1201:ALESIS>2.0.CO;2)
- Slade, J.H., Thalman, R., Wang, J. & Knopf, D.A. (2015) Chemical aging of single and multicomponent biomass burning aerosol surrogate particles by OH: implications for cloud condensation nucleus activity. *Atmospheric Chemistry and Physics*, 15, 10183–10201. <https://doi.org/10.5194/acp-15-10183-2015>
- Storer, R.L. & van den Heever, S.C. (2013) Microphysical processes evident in aerosol forcing of tropical deep convective clouds. *Journal of the Atmospheric Sciences*, 70(2), 430–446. <https://doi.org/10.1175/JAS-D-12-076.1>
- Tanner, R.L. & Newman, L. (1976) The analysis of airborne sulfate. *Journal of the Air Pollution Control Association*, 26(8), 737–747. <https://doi.org/10.1080/00022470.1976.10470308>
- Tiwari, M., Sahu, S.K., Bhangare, R.C., Yousaf, A. & Pandit, G. G. (2014) Particle size distributions of ultrafine combustion aerosols generated from household fuels. *Atmospheric Pollution Research*, 5, 145–150. <https://doi.org/10.5094/APR.2014.018>

- U.S. Geological Survey. (2013) Landsat 8 OLI (Operational Land Imager), Level 1. <https://doi.org/10.5066/F71835S6> [Accessed 30th March 2022].
- US EPA. (2012) *First quarter, reducing black carbon emissions in South Asia report*. Washington, DC: US EPA, p. 10. <https://nepis.epa.gov/Exe/ZyPURL.cgi?Dockey=P100EF3D.TXT> [Accessed 30th March 2022].
- Varun Raj, S., Ghosh, S. & Sivakumar, B. (2009) Aerosol growth and activation in polluted air masses over a tropical metropolis in the Indian sub-continent. *Atmospheric Science Letters*, 10(2), 66–74. <https://doi.org/10.1002/asl.212>
- Wong, J.P.S., Lee, A.K.Y., Slowik, J.G., Cziczo, D.J., Leaitch, W.R., Macdonald, A. et al. (2011) Oxidation of ambient biogenic secondary organic aerosol by hydroxyl radicals: effects on cloud condensation nuclei activity. *Geophysical Research Letters*, 38, L22805. <https://doi.org/10.1029/2011GL049351>
- Yamasoe, M.A., Artaxo, P., Miguel, A.H. & Allen, A.G. (2000) Chemical composition of aerosol particles from direct emissions of vegetation fires in the Amazon Basin: water-soluble species and trace elements. *Atmospheric Environment*, 34(10), 1641–1653. [https://doi.org/10.1016/S1352-2310\(99\)00329-5](https://doi.org/10.1016/S1352-2310(99)00329-5)

- Young, S.A. & Vaughan, M.A. (2009) The retrieval of profiles of particulate extinction from cloud-aerosol lidar infrared pathfinder satellite observations (CALIPSO) data: algorithm description. *Journal of Atmospheric and Oceanic Technology*, 26, 1105–1119. <https://doi.org/10.1175/2008JTECHA1221.1>

SUPPORTING INFORMATION

Additional supporting information can be found online in the Supporting Information section at the end of this article.

How to cite this article: Ghosh, S., Sathish Kumar, C. R., Gumber, S., Dobbie, S., & Yang, H. (2022). How Asian slum emissions impact local microclimates in polluted air masses. *Atmospheric Science Letters*, 23(12), e1124. <https://doi.org/10.1002/asl.1124>